International Journal of QUANTUM CHEMISTRY WWW.Q-CHEM.ORG FULL PAPER

The Orbital Overlap Distance in Graphene Defects

Arshad Mehmood[1] and Benjamin G. Janesko[1]

Correspondence to: Arshad Mehmood (E-mail: *arshad.mehmood@tcu.edu*)

[1] Department of Chemistry & Biochemistry, Texas Christian University, 2800 South University Drive, Fort Worth, TX 76129, USA.

ABSTRACT

Quantum-chemical "descriptors", including atomic partial charges, orbitals, and electrostatic potentials are powerful tools for understanding chemical reactivity. Localized defects in graphene are a particular challenge for these tools, especially to model the adsorption processes and to predict the interactions of transition metals with these defects. Such defects often have little charge polarization and a combination of localized and delocalized states. Our orbital overlap distance D(**r**) measures the "size" of occupied orbital lobes about point **r**, distinguishing the hybridization state and compact *vs.* diffuse character of local electronic structure. Here we apply the overlap distance to graphene defects. We find that the overlap distance clearly distinguishes differential reactivities of different atoms at intrinsic defects. Combining the overlap distance and electrostatic potential provides a rich picture of extrinsic defect reactivity, including semiquantitative predictions of transition metal binding.

Introduction

Structural defects in graphene open the bandgap and allow catalysts and intermediates to bind to the surface.[1-5] These defects alter graphene's chemical reactivity[1,6,7] and electronic structure,[8-11] induce magnetism[12-15] and reduce electron mobility[16,17], Young modulus[18,19] and Poisson ratio[20]. These defects can appear during production and growth or can be incorporated by post-processing particle (electron and ion beam) irradiation and chemical methods termed as chemical functionalization.[1,9,21-23] Foreign adatoms, which interact with graphene either by van der Waals interactions (physisorption), chemical bonds (chemisorption) or as substitutional impurities, have received considerable attention due to their ability to act as catalysts (*e.g.* transition metals) or due to the controlled alterations in electrical conductivity and electronic structure of graphene (*e.g.* boron or nitrogen doping).[1,23,24] Adatoms often bind to graphene at defects, particularly at the vacant sites of vacancy defects.[25] The control of the location of Stone – Wales (SW) and vacancy defects, type of dopant and adatoms pave the way towards the preparation of new graphene-based materials with novel physical and chemical properties.[9,26,27] Chemically, the doping can enhance its reactivity as catalyst, as diene or dienophile in Diels-Alder, in aerobic oxidations, oxidative dehydrogenations and cycloaddition reactions.[23,28-32] The vacancy defects which have high spatial selectivity, adsorbed and adatoms transition metals can turn the defective site into a single atom catalyst.[4,33-35]

Understanding the physical and chemical consequences of graphene defects and their interactions with dopants requires the understanding of defect's atomic and electronic structure.[36] Computed "descriptors" of

electronic structure can often provide such understanding from relatively simple calculations. (To illustrate, the pK_a of a compound could be computed from extensive *ab initio* molecular dynamics simulations in explicit solvent, however computed atomic partial charges often provide a much more readily computed prediction of relative pK_a.) Simulated molecular electrostatic potentials (ESP) and atomic partial charges (Q_A) are widely used to predict and interpret the chemical reactivity of molecules, solids, surfaces, and nanoparticles.[37,38] However, these descriptors are often insufficient for materials like carbon allotropes. For example, pristine graphene, diamond, and C_{60} all have atomic partial charge of zero (Table 1), but possess different reactivities and heat of formations.[39]

Intrinsic defects in graphene often combine relatively large variations in chemical reactivity with relatively insignificant variations in ESP or atomic partial charges. Chemically, all of the atoms in an intrinsic defect have the same electronegativity. To illustrate, we consider the single vacancy (V_1), double vacancy (V_2), and Stone-Wales (SW) defects shown in Figure 1. Figure 1 and Table 2 show that these defects have relatively small variations in ESP and atomic charges. However, previous studies have clearly demonstrated that these different defects have different chemistry. These defects show markedly different binding energies to H_2OH, H_2OCO, NO, –H, –F and –Ph groups.[6,40] These defects also show different adsorption energies for transition metal atoms, even atoms with similar charge and ionic radius.[34,41] The pentagons of V_2 and SW are more prone to oxidation, while the octagons prefer reduction and provide favorable sites for radical attacks.[42] Extrinsic defects in graphene can also combine large variations in chemical reactivity with small variations in electrostatics. Nitrogen and phosphorus dopants both give comparable changes to graphene's computed ESP, however phosphorus lowers the activation energy for cycloaddition and favors [4+2] over [2+2] cycloadditions.[43]

There have been many efforts to quantify aspects of graphene reactivity missing from partial atomic charges and ESP. Frontier orbitals analysis[44] and conceptual density functional theory (DFT)[45] based descriptors such as reactivity indices[45-47] and Fukui functions[42,48-51] *etc.,* have been used to compliment the atomic partial charges. However, previous studies have demonstrated that these method are strongly dependent on the basis set and exchange correlation potential used in DFT calculations.[45,52] In addition, frontier orbitals and conceptual DFT quantifies global properties only and these methods struggle to distinguish the local chemistry of different sites on a single molecule.[45,46,53] We have developed a descriptor of electronic structure that complements atomic partial charges and ESP, characterizing the hybridization and localization of orbitals as distinct from the polarization of charge. Our orbital overlap distance function, D(**r**), quantifies whether the occupied orbital *lobes* around point **r** are small and compact or large and diffuse.[39,54-56] D(**r**) is constructed from the one-particle reduced density matrix $\gamma(\mathbf{r},\mathbf{r}') = \sum_{\mathrm{i}} n_{\mathrm{i}}\,\psi_{\mathrm{i}}(\mathbf{r})\psi_{\mathrm{i}}(\mathbf{r}')$ of molecular orbitals ψ_{i} with nonzero occupancy, n_{i}. At each point **r**, we project the orbitals onto an *s*-orbital-like test function $\mathrm{C}_d \exp\left(-\frac{|\mathbf{r}-\mathbf{r}'|^2}{d^2}\right)$ centered at point **r** and having width *d*:

$$\mathrm{EDR}(\mathbf{r};d) = \rho^{-\frac{1}{2}}(\mathbf{r}) \int \mathrm{d}^3\mathbf{r}'\gamma(\mathbf{r},\mathbf{r}')\mathrm{C}_d \exp\left(-\frac{|\mathbf{r}-\mathbf{r}'|^2}{d^2}\right)$$

The orbital overlap distance D(**r**) is the distance d, which maximizes this quantity at point **r**: $\mathrm{D}(\mathbf{r}) = \underset{d}{\mathrm{argmax}}\ \mathrm{EDR}(\mathbf{r}; d)$. Atom averaged overlap distance D_A is:

$$\mathrm{D_A} = \frac{1}{N_\mathrm{A}} \int d^3\mathbf{r}\, w_\mathrm{A}(\mathbf{r}) \rho(\mathbf{r}) \mathrm{D}(\mathbf{r})$$

D_A and plots of D(**r**) on electron density isosurfaces provide orbital information that complement atomic partial charges and electrostatic potentials.[39] For example, atom averaged D_C for carbon allotropes (Table 1) decrease as C_{atom} > C_{60} > graphene > diamond, mirroring to some extent the relative thermodynamic stability and providing information where atomic partial charges cannot. We have applied these tools to capture trends in aromaticity, nucleophilicity, allotrope stability, and substituent effects.[39,54]

The considerations discussed above suggest that the orbital overlap difference could be particularly well-suited to understanding the chemistry of graphene intrinsic and extrinsic defects. We find that differences in hybridization and diffuseness at defect sites [39] correlate with the relative reactivity of individual atoms at defect sites. The overlap distance thus provides a useful new perspective on the site-dependent reactivity of graphene defects.

Table 1. Charge Q_C and atomic overlap distance D_C of carbon atom in representative allotropes.

Allotrope	Q_C (e)	D_C (bohr)
Diamond	0.00	1.54
Graphene	0.00	1.58
C60	0.00	1.60
Isolated C atom	0.00	2.12

Computational Details

We model all defects as finite zero-dimensional hydrogen-capped graphene flakes. Most of our calculations introduce defects into a polybenzenoid hydrocarbon $C_{96}H_{24}$ containing 37 fused benzene rings. Previous studies have validated this as a model for local defects.[82] For transition metal adatoms, we selected a smaller graphene flake for which the adsorption energies have been reported.[16] Electronic structure calculations use the Gaussian 09[57] suite of programs. We report geometries optimized with density functional theory (DFT) using the (U)M06-2X[58] level of theory with the 6-31G(d) basis set. Single-point energy calculations were subsequently carried on the optimized structures at the (U)M06-2X level with the larger basis set 6-311G(d,p). For transition metal atoms, the calculations were performed using def2-TZVP[59] basis set. The obtained formatted check-point files of Gaussian were used as input for Multiwfn[60] program to calculate, density, D(**r**) and ESP Gaussian cube file format. The same program was used to calculate both D_A and Q_A using Hirshfeld partitioning scheme. Our implementations to Multiwfn[60] program determine weight $w_\mathrm{A}(\mathbf{r})$ assigned to an atom A in the molecule using the Hirshfeld, Voronoi, Becke and Hirshfeld-I partitioning schemes.

Results and Discussion

Intrinsic Defects

We begin by considering vacancy and Stone-Wales intrinsic defects. Figure 1 compares the ESP and overlap distance, D(**r**), evaluated on the 0.001 electrons/bohr^3 density isosurface. Table 2 shows the corresponding atom-averaged quantities. Supporting information Figure S1 shows similar plots for defect free/pristine graphene surface. Figure S2 shows the computed HOMO and LUMO plots. As discussed above, the electrostatic potential at the defect

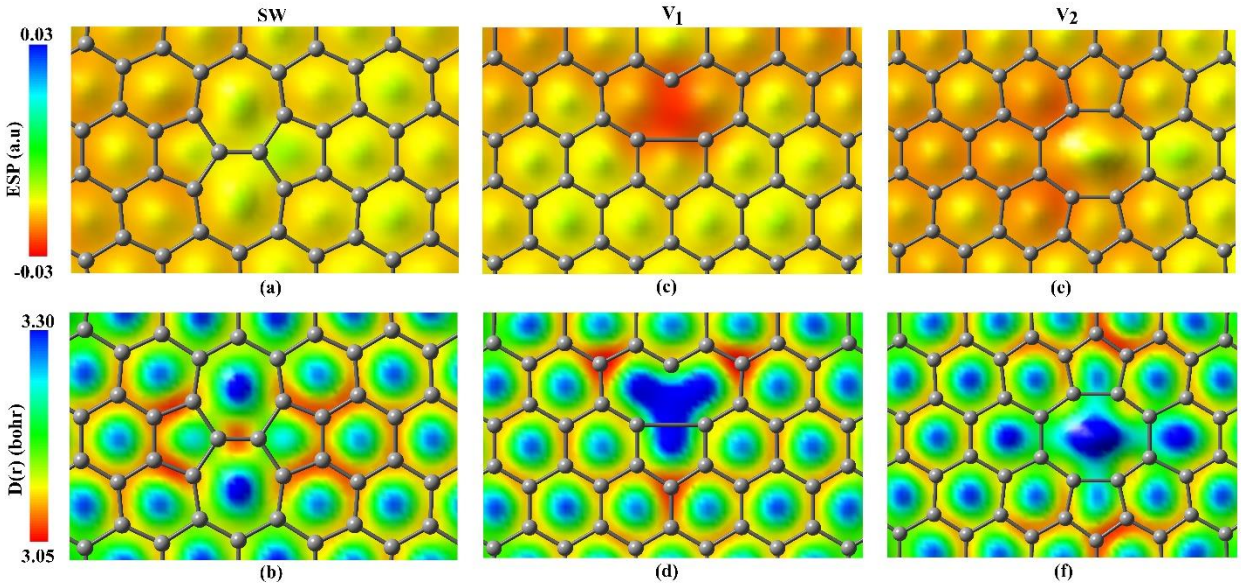

Figure 1 0.001 e/bohr^3 density isosurface plots of ESP for SW, reconstructed V_1 and V_2 defects. The bottom of figure represents similar density isosurface plots of D(**r**) for these defects distinguishing the regions on surface with compact orbitals of small D(**r**) (red) from the regions which have more diffuse orbitals showing large values of D(**r**) (blue).

sites differ little from the surrounding graphene.

Inspection of the D(**r**) plots in Figure 1b shows a much richer chemistry. D(**r**) is relatively small in the π system, consistent with the *p*-orbital character of the π orbitals, and is relatively large in the aromatic ring centers matching our previous results.[39] More importantly, the orbital overlap distance clearly distinguishes the carbon atoms of SW pentagons *vs*. heptagons. The pentagons possess smaller orbital lobes consistent with chemically "harder" behavior. Similarly, the hollow site of heptagons has large value of D(**r**) as compared to the hollow site of pentagons and the junction of these pentagons has relatively small D(**r**).

As in our previous work, combining the ESP and the overlap distance gives a rich and experimentally relevant picture of defect chemistry.[39] The computed ESP of V_1 defect (Figure 1c), shows that the hollow site of the nine-member ring has negative ESP, making it a relatively *basic* region on the graphene surface. The most basic site is the radical/unsaturated carbon atom. The corresponding D(**r**) (Figure 1d) shows that the occupied orbital lobes around

Table 2. Calculated Hirshfeld charges Q_A (e) and atomic overlap distance D_A (bohr) for selected atoms (labelled in figure) of defected graphene systems relative to the central carbon atom of pristine graphene.

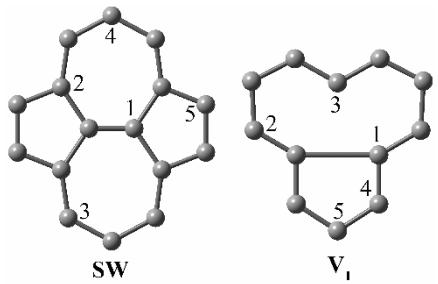

Atom	SW		V_1	
	Q_A	D_A	Q_A	D_A
C1	0.021	1.000	0.024	1.062
C2	-0.016	1.002	-0.006	1.005
C3	0.016	1.017	0.021	1.060
C4	-0.006	1.016	-0.007	1.004
C5	-0.017	0.981	-0.023	0.996

this site are relatively large and diffuse, with a large D(**r**). Combined, these results suggest that the V_1 defect has *soft basic* character. The ESP of V_2 defects (Figure 1e) shows that the octagonal hollow site has more positive ESP, making it a relatively acidic site on the graphene surface. The corresponding D(**r**) is again rather large, suggesting that the V_2 defect has *soft acidic* character. These predictions prove to be consistent with the literature. Chemically soft transition metal cations show relatively strong adsorption to the graphene V_1 defect.[61] Relatively soft transition metals such as Ag, Au, and Pt show 4 times enhanced stability on V_2 *vs*. on pristine graphene, whereas relatively hard metals such as Li show already strong binding to pristine graphene and insignificant enhancement in stability on V_2 *vs*. pristine graphene.[62] Note that the defect HOMO and LUMO (Figure S2) only provides a global picture and cannot distinguish the site-dependent reactivity. We next demonstrate how combining atom-averaged charges and overlap distance D_A distinguishes the reactivity of each carbon atom at defect sites. Table 2 presents calculated Hirshfeld charges and D_A of selected carbon atoms of SW and V_1 defects.

We first consider the Stone-Wales defect. Atom C4 is slightly negative and has relatively large value of D_A, consistent with *soft basic* character. Atom C5 has the most negative charge and lowest value of D_A, consistent with *hard basic* character. Similarly, atom C1 is a "*hard acidic*" while atom C3 is a "*soft acidic*" site. These findings suggest that soft and hard acidic reagents will prefer sites C4 and C5 respectively. Similarly, hard and soft basic species will prefer SW sites C1 and C3 respectively. These predictions for Stone-Wales defect reactivity concur with other quantum mechanical descriptors[42] and are consistent with the literature. Chemically *hard* radicals such as F, Ph and COOH prefer SW site C1 for chemisorption.[6,40,42] Metal atoms preferentially adsorb to SW heptagons (C2) over pentagons (C5) despite their similar charges.[63]

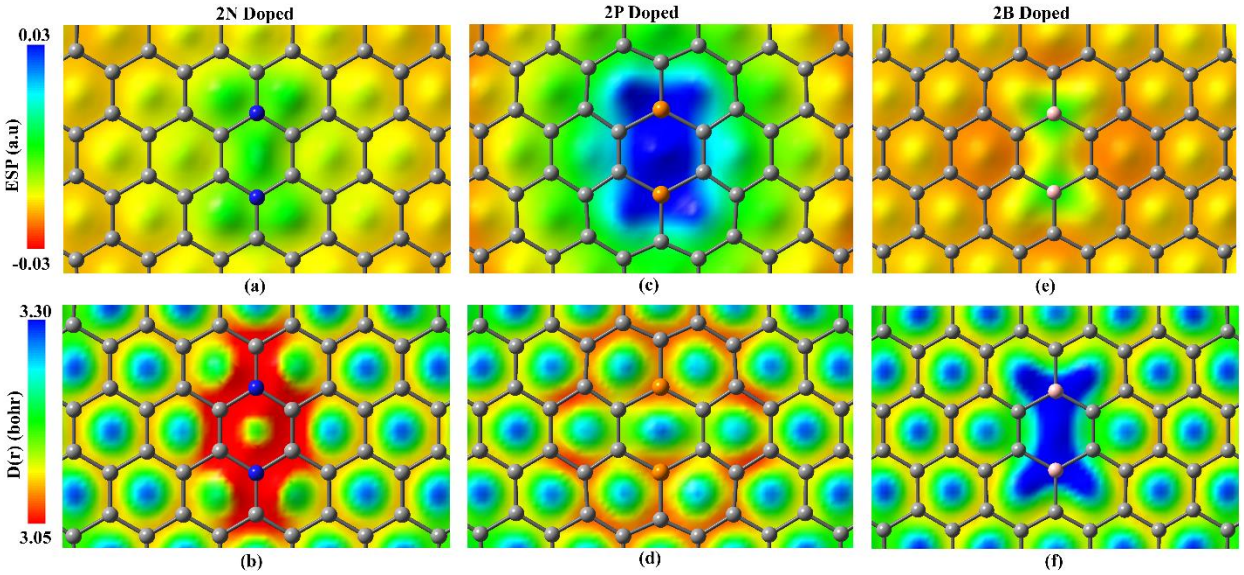

Figure 2 0.001 e/bohr^3 density isosurface plots of ESP for 2N (a), 2P (c) and 2B (e) doped graphene sheet. The bottom of figure represents similar density isosurface plots of D(**r**) for these doped systems distinguishing the regions on surface with compact orbitals of small D(**r**) (red) from the regions which have more diffuse orbitals showing large values of D(**r**) (blue).

We next consider the V_1 defect. Here atom C1 has the most positive charge and largest D_A, consistent with soft acidic character. Atom C5 has the most negative charge and lowest D_A, consistent with hard basic character. Atom C3 has a dangling bond giving again a relatively large D_A. This is broadly consistent with the literature, with the V_1 defect reactivity dominated by the dangling bond on C3.[64]

Extrinsic Defects

We next consider the orbital overlap distance for extrinsic substitutional defects. Figure 2 compares the ESP and D(**r**) evaluated on the 0.001 electrons/bohr^3 density isosurface for defects where two carbon atoms are substituted with nitrogen, phosphorus, or boron respectively. Figure S3 shows a similar plot for graphene sheet containing two silicon atoms. For these systems the dopant atoms lie in the graphene plane. These extrinsic defects yield larger charge polarization and larger variations in the surface ESP. Nitrogen is electron withdrawing and give a net positive charge in the graphene π system (Figure 2a, Mulliken charges -0.9e on nitrogen, ~0.4e on adjacent carbon atoms). Phosphorus and boron are electron donating, consistent with their electronegativities lower than carbon, and give a net negative charge in the graphene π system. Similar effects were previously seen for phosphorus dopants.[67] Phosphorus doping gives Mulliken charges +1.3e on phosphorus, -0.5e to -0.8e on adjacent carbon atoms. The orbital overlap distance also shows large differences between nitrogen, phosphorus and boron dopants. The compact and electron-withdrawing nitrogen dopants make the overlap distance relatively small both at nitrogen and at adjacent carbon atoms (Figure 2b). (Physically, charge and overlap distance often show an inverse relation. When electron density is removed from an atom increasing its partial charge, the remaining electrons are held relatively tightly, reducing the overlap distance.) Carbon atoms near an N dopant are relatively "*hard*" compared to pristine graphene. The electron-donating phosphorus dopants also make the overlap distance slightly smaller near the defect, consistent with the more positive charge (Figure 2d). In contrast, boron dopants dramatically increase the overlap distance, despite the overall positive electrostatic potential (Figure 2f). Similar trends occur for silicon dopants (Figure S3). Broadly speaking, nitrogen doping gives a "*hard*" basic site, phosphorous doping gives a relatively strong acidic site with intermediate *"hardness*", and boron and silicon doping generate relatively "*soft*" acidic sites. These results compliment the literature, which finds that [2+2] cycloaddition of hard reagents like

Table 3 Trends in transition metal binding. First column shows the atomic radius[65], second and third columns represent surface electrostatic potential and surface overlap distance of isolated neutral transition metal atoms calculated at 0.001 e/bohr^3 density isosurface. Fourth column show the computed binding energies to V_1 defects relative to bulk metal taken from ref. [66].

Metal	Atomic Radius (Å)	Surface ESP (a.u)	Surface D(**r**) (bohr)	V_1 B.E (kJ/mol)
Ni	1.24	0.007	2.096	-201
Co	1.26	0.015	5.976	-267
Fe	1.32	0.018	5.890	-235
Cu	1.32	0.009	5.588	-267
Pt	1.36	0.005	2.256	-187
Au	1.36	0.006	4.161	54
Cr	1.39	0.013	6.092	-221
Pd	1.39	0.005	2.186	-160
Ir	1.41	0.018	5.731	-201
Rh	1.42	0.012	2.497	-254

benzene is preferred for 2N doped over 2B and 2Si doped graphene.[43]

Transition Metal Binding

We conclude by considering transition metal adsorption to vacancy defects. Previous computational studies have shown rather complex trends, with binding to V_1 defects generally more favorable than formation of bulk metal.[66] Table 3 illustrates that orbital effects are particularly important for binding. Pairs of transition metal atoms possessing similar atomic radius and surface electrostatic potential can have very different V_1 binding energies. (Examples include Ni and Co, Fe and Cu, or Pt and Au.) *Remarkably, in most cases, atoms with a larger value of the surface overlap distance tend to bind stronger to V_1*. This nontrivial prediction allows us to predict V_1 binding from a simulation of only the isolated metal atom. Figure 3 rationalizes why the surface overlap distance is useful. The surface overlap distances in Figure 3 form two trendlines, corresponding to "*s*-valent" and "*d*-valent" metals. The "*s*-valent" metals with larger surface overlap distance have an *s*-type highest occupied atomic orbital. Examples include isolated spin quintet Fe with electronic configuration $[Ar]3d^6 4s^2$, and isolated spin-doublet Au with electronic configuration $[Xe]4f^{14}5d^{10}6s^1$.

The "*d*-valent" metals with smaller surface overlap distance have a *d*-type highest occupied atomic orbital. Examples include isolated spin-singlet nickel atom with electronic configuration $[Ar]3d^8 4s^2$. Within these groups, atoms with a relatively large surface overlap distance give relatively large binding to V_1. For example, "*d*-valent" Pd, Pt, and Rh have D_{surf} increase 2.18, 2.25, 2.49 bohr and have V_1 binding increase -160, -187, -254 kJ/mol. Similarly, "*s*-valent" Mo, Ir, Fe have D_{surf} increase 5.20, 5.73, 5.89 bohr and have V_1 binding increase -112, -201, -235 kJ/mol respectively.

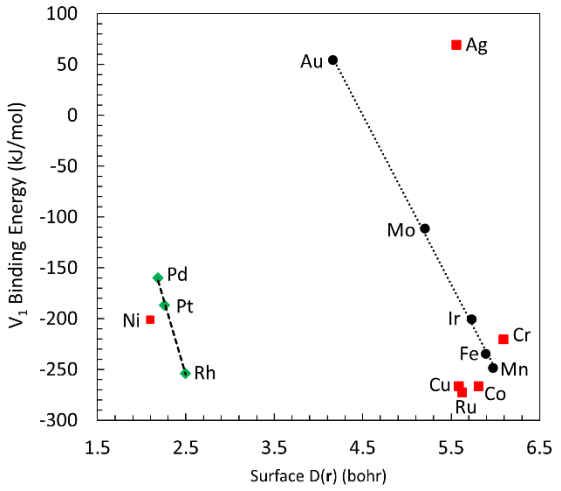

Figure 3 Relation between binding energies of some selected transition metals atoms on V_1 defect and surface D(**r**) calculated at 0.001 e/bohr^3 density isosurface. The outliers are shows using red squares. Table S1 provides the atomic radius, calculated ESP, D(**r**) and binding energies of these metals.

We close by demonstrating the overlap distance for an adsorbed metal. Figure 4 shows the surface overlap distance for cobalt, iron, and manganese adsorbed to a V_1 vacancy defect. The overlap distance is relatively large on the cobalt atom and smaller on iron and manganese. Similar trends occur for the carbons near the transition metal. In terms of electrostatics, the calculated charges of the bound metal are 0.02e for cobalt, 0.32e for iron, and 0.39e for manganese. Overall, adsorbed cobalt provides a comparatively "*soft*" weak acid site. Iron and manganese provide "*harder*" and more acidic sites. These results are consistent with the observation that cobalt single atom catalysts preferentially bind "*soft*" H_2, whereas manganese shows higher selectivity for binding "*harder*" CO.[34,68]

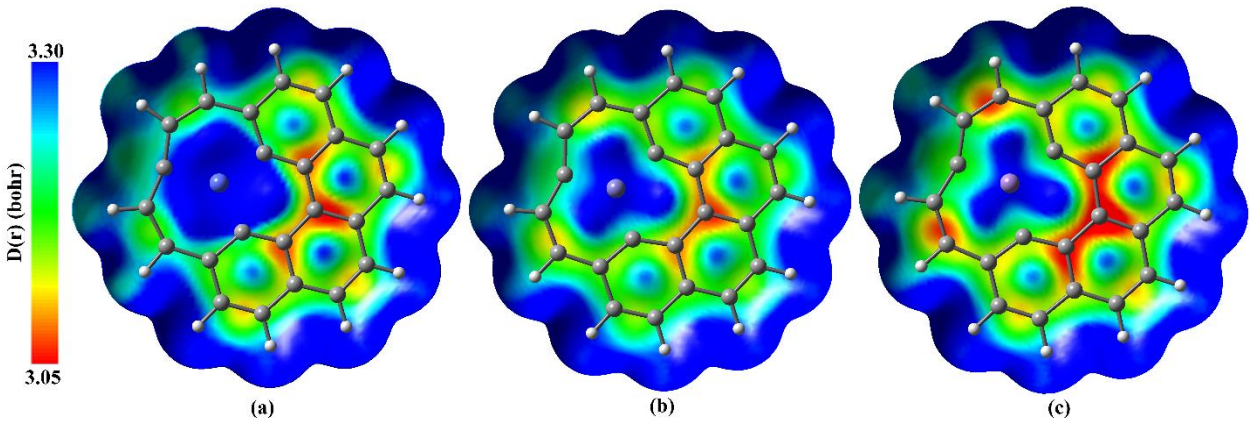

Figure 4 Plots of D(**r**) on 0.001 e/bohr^3 electron density isosurface for chemisorbed transition metal atoms (a) Co (b) Fe (c) Mn at the V_1 defect site of graphene nano flakes.

Conclusions

We show that the orbital overlap distance provides a useful complement to electrostatic potentials for visualizing and interpreting the reactivity of graphene defects. The overlap distance is particularly useful for intrinsic defects, whose large variations in reactivity generally do not produce large variations in electrostatics. Combining the overlap distance with electrostatic potentials gives a richer picture of reactivity in extrinsic defects. The computed overlap distances of isolated metal atoms also prove to give insights into their adsorption to graphene defects. Overall, these results motivate further applications of the overlap distance to understanding defect chemistry.

Keywords: Graphene, Defects, Overlap distance, Molecular Modelling, Hard-Soft

Additional Supporting Information may be found in the online version of this article.

References

1. Banhart, F.; Kotakoski, J.; Krasheninnikov, A. V. ACS Nano 2011, 5, 26-41.
2. Eftekhari, A.; Garcia, H. Mater Today Chem 2017, 4, 1-16.
3. Raccichini, R.; Varzi, A.; Passerini, S.; Scrosati, B. Nat Mater 2014, 14, 271.
4. Jia, Y.; Zhang, L.; Du, A.; Gao, G.; Chen, J.; Yan, X.; Brown, C. L.; Yao, X. Adv Mater 2016, 28, 9532-9538.
5. Xu, X.; Liu, C.; Sun, Z.; Cao, T.; Zhang, Z.; Wang, E.; Liu, Z.; Liu, K. Chem Soc Rev 2018, 47, 3059-3099.
6. Denis, P. A.; Iribarne, F. J Phys Chem C 2013, 117, 19048-19055.
7. Bellunato, A.; Arjmandi Tash, H.; Cesa, Y.; Schneider, G. F. ChemPhysChem 2016, 17, 785-801.
8. Son, Y.-W.; Cohen, M. L.; Louie, S. G. Nature 2006, 444, 347-349.
9. Robertson, A. W.; Allen, C. S.; Wu, Y. A.; He, K.; Olivier, J.; Neethling, J.; Kirkland, A. I.; Warner, J. H. Nat Commun 2012, 3, 1144.
10. Cantele, G.; Lee, Y.-S.; Ninno, D.; Marzari, N. Nano Lett 2009, 9, 3425-3429.
11. Ugeda, M. M.; Brihuega, I.; Hiebel, F.; Mallet, P.; Veuillen, J.-Y.; Gómez-Rodríguez, J. M.; Ynduráin, F. Phys Rev B 2012, 85, 121402.
12. Ma, Y.; Lehtinen, P. O.; Foster, A. S.; Nieminen, R. M. New J Phys 2004, 6, 68-68.
13. Lehtinen, P. O.; Foster, A. S.; Ma, Y.; Krasheninnikov, A. V.; Nieminen, R. M. Phys Rev Lett 2004, 93, 187202.

14. Yazyev, O. V.; Helm, L. Phys Rev B 2007, 75, 125408.
15. Pidatella, A.; Mazzarello, R. In Correlations in Condensed Matter under Extreme Conditions: A tribute to Renato Pucci on the occasion of his 70th birthday; Angilella, G. G. N.; La Magna, A., Eds.; Springer International Publishing: Cham, 2017, p 195-214.
16. Ni, Z. H.; Ponomarenko, L. A.; Nair, R. R.; Yang, R.; Anissimova, S.; Grigorieva, I. V.; Schedin, F.; Blake, P.; Shen, Z. X.; Hill, E. H.; Novoselov, K. S.; Geim, A. K. Nano Lett 2010, 10, 3868-3872.
17. Chen, J.-H.; Cullen, W. G.; Jang, C.; Fuhrer, M. S.; Williams, E. D. Phys Rev Lett 2009, 102, 236805.
18. Jing, N.; Xue, Q.; Ling, C.; Shan, M.; Zhang, T.; Zhou, X.; Jiao, Z. RSC Adv 2012, 2, 9124-9129.
19. Thomas, S.; Mrudul, M. S.; Ajith, K. M.; Valsakumar, M. C. J Phys: Conf Ser 2016, 759, 012048.
20. Dettori, R.; Cadelano, E.; Colombo, L. J Phys: Condens Matter 2012, 24, 104020.
21. Kotakoski, J.; Meyer, J. C.; Kurasch, S.; Santos-Cottin, D.; Kaiser, U.; Krasheninnikov, A. V. Phys Rev B 2011, 83, 245420.
22. Pantelides, S. T.; Puzyrev, Y.; Tsetseris, L.; Wang, B. MRS Bull 2012, 37, 1187-1194.
23. Boukhvalov, D. W.; Katsnelson, M. I. Nano Lett 2008, 8, 4373-4379.
24. Ci, L.; Song, L.; Jin, C.; Jariwala, D.; Wu, D.; Li, Y.; Srivastava, A.; Wang, Z. F.; Storr, K.; Balicas, L.; Liu, F.; Ajayan, P. M. Nat Mater 2010, 9, 430.
25. Cretu, O.; Krasheninnikov, A. V.; Rodríguez-Manzo, J. A.; Sun, L.; Nieminen, R. M.; Banhart, F. Phys Rev Lett 2010, 105, 196102.
26. Lahiri, J.; Lin, Y.; Bozkurt, P.; Oleynik, I. I.; Batzill, M. Nat Nanotechnol 2010, 5, 326.
27. Carr, L. D.; Lusk, M. T. Nat Nanotechnol 2010, 5, 316.
28. Sarkar, S.; Bekyarova, E.; Niyogi, S.; Haddon, R. C. Journal of the American Chemical Society 2011, 133, 3324-3327.
29. Cao, Y.; Osuna, S.; Liang, Y.; Haddon, R. C.; Houk, K. N. Journal of the American Chemical Society 2013, 135, 17643-17649.
30. Denis, P. A. Chem Eur J 2013, 19, 15719-15725.
31. Navalon, S.; Dhakshinamoorthy, A.; Alvaro, M.; Garcia, H. Chem Rev 2014, 114, 6179-6212.
32. Qi, W.; Su, D. ACS Catal 2014, 4, 3212-3218.
33. Sahoo, S.; Suib, S. L.; Alpay, S. P. ChemCatChem 2018, 10, 3229-3235.
34. Xu, L.; Yang, L.-M.; Ganz, E. Theor Chem Acc 2018, 137, 98.
35. Ito, Y.; Cong, W.; Fujita, T.; Tang, Z.; Chen, M. Angew Chem 2015, 127, 2159-2164.
36. Pykal, M.; Jurečka, P.; Karlický, F.; Otyepka, M. Physical Chemistry Chemical Physics 2016, 18, 6351-6372.
37. Marenich, A. V.; Jerome, S. V.; Cramer, C. J.; Truhlar, D. G. J Chem Theory Comput 2012, 8, 527-541.
38. Over, H.; Kim, Y. D.; Seitsonen, A. P.; Wendt, S.; Lundgren, E.; Schmid, M.; Varga, P.; Morgante, A.; Ertl, G. Science 2000, 287, 1474.
39. Mehmood, A.; Janesko, B. G. Angew Chem Int Ed 2017, 56, 6878-6881.
40. OuYang, F.; Huang, B.; Li, Z.; Xiao, J.; Wang, H.; Xu, H. J Phys Chem C 2008, 112, 12003-12007.
41. Wan, W.; Wang, H. Mater Corros 2015, 8, 163-6178.
42. Kudur Jayaprakash, G.; Casillas, N.; Astudillo-Sánchez, P. D.; Flores-Moreno, R. J Phys Chem A 2016, 120, 9101-9108.
43. Denis, P. A. ChemistrySelect 2016, 1, 5497-5500.
44. Haldar, S.; Kolář, M.; Sedlák, R.; Hobza, P. J Phys Chem C 2012, 116, 25328-25336.
45. Geerlings, P.; De Proft, F.; Langenaeker, W. Chem Rev 2003, 103, 1793-1874.
46. Anderson, J. S. M.; Melin, J.; Ayers, P. W. J Chem Theory Comput 2007, 3, 358-374.
47. Peralta-Inga, Z.; Murray, J. S.; Edward Grice, M.; Boyd, S.; O'Connor, C. J.; Politzer, P. Journal of Molecular Structure: THEOCHEM 2001, 549, 147-158.
48. Hernández Rosas, J. J.; Ramírez Gutiérrez, R. E.; Escobedo-Morales, A.; Chigo Anota, E. J Mol Model 2011, 17, 1133-1139.

49. Cortés Arriagada, D. J Mol Model 2013, 19, 919-930.
50. Kudur Jayaprakash, G.; Swamy, B. E. K.; Casillas, N.; Flores-Moreno, R. Electrochim Acta 2017, 258, 1025-1034.
51. Jayaprakash, G. K.; Flores-Moreno, R. Electrochim Acta 2017, 248, 225-231.
52. Shankar, R.; Senthilkumar, K.; Kolandaivel, P. Int J Quantum Chem 2009, 109, 764-771.
53. Berger, G. Comp Theor Chem 2013, 1010, 11-18.
54. Janesko, B. G.; Wiberg, K. B.; Scalmani, G.; Frisch, M. J. J Chem Theory Comput 2016, 12, 3185-3194.
55. Janesko, B. G.; Scalmani, G.; Frisch, M. J. Physical Chemistry Chemical Physics 2015, 17, 18305-18317.
56. Mehmood, A.; Jones, S. I.; Tao, P.; Janesko, B. G. J Chem Inf Model 2018, 58, 1836-1846.
57. Frisch, M. J.; Trucks, G. W.; Schlegel, H. B.; Scuseria, G. E.; Robb, M. A.; Cheeseman, J. R.; Scalmani, G.; Barone, V.; Mennucci, B.; Petersson, G. A.; Nakatsuji, H.; Caricato, M.; Li, X.; Hratchian, H. P.; Izmaylov, A. F.; Bloino, J.; Zheng, G.; Sonnenberg, J. L.; Hada, M.; Ehara, M.; Toyota, K.; Fukuda, R.; Hasegawa, J.; Ishida, M.; Nakajima, T.; Honda, Y.; Kitao, O.; Nakai, H.; Vreven, T.; Montgomery Jr., J. A.; Peralta, J. E.; Ogliaro, F.; Bearpark, M. J.; Heyd, J.; Brothers, E. N.; Kudin, K. N.; Staroverov, V. N.; Kobayashi, R.; Normand, J.; Raghavachari, K.; Rendell, A. P.; Burant, J. C.; Iyengar, S. S.; Tomasi, J.; Cossi, M.; Rega, N.; Millam, N. J.; Klene, M.; Knox, J. E.; Cross, J. B.; Bakken, V.; Adamo, C.; Jaramillo, J.; Gomperts, R.; Stratmann, R. E.; Yazyev, O.; Austin, A. J.; Cammi, R.; Pomelli, C.; Ochterski, J. W.; Martin, R. L.; Morokuma, K.; Zakrzewski, V. G.; Voth, G. A.; Salvador, P.; Dannenberg, J. J.; Dapprich, S.; Daniels, A. D.; Farkas, Ö.; Foresman, J. B.; Ortiz, J. V.; Cioslowski, J.; Fox, D. J.; Gaussian, Inc.: Wallingford, CT, USA, 2009.
58. Zhao, Y.; Truhlar, D. G. Theor Chem Acc 2008, 120, 215-241.
59. Weigend, F.; Ahlrichs, R. Physical Chemistry Chemical Physics 2005, 7, 3297-3305.
60. Lu, T.; Chen, F. J Comput Chem 2012, 33, 580-592.
61. Pašti, I. A.; Jovanović, A.; Dobrota, A. S.; Mentus, S. V.; Johansson, B.; Skorodumova, N. V. Physical Chemistry Chemical Physics 2018, 20, 858-865.
62. Fair, K. M.; Cui, X. Y.; Li, L.; Shieh, C. C.; Zheng, R. K.; Liu, Z. W.; Delley, B.; Ford, M. J.; Ringer, S. P.; Stampfl, C. Phys Rev B 2013, 87, 014102.
63. Zhou, L.-J.; Hou, Z. F.; Wu, L.-M. J Phys Chem C 2012, 116, 21780-21787.
64. Gürel, H. H.; Özçelik, V. O.; Ciraci, S. J Phys Chem C 2014, 118, 27574-27582.
65. Cordero, B.; Gómez, V.; Platero-Prats, A. E.; Revés, M.; Echeverría, J.; Cremades, E.; Barragán, F.; Alvarez, S. Dalton Transactions 2008, 2832-2838.
66. Kropp, T.; Mavrikakis, M. ACS Catal 2019, 6864-6868.
67. Esrafili, M. D.; Mohammad-Valipour, R.; Mousavi-Khoshdel, S. M.; Nematollahi, P. ChemPhysChem 2015, 16, 3719-3727.
68. Jiang, K.; Siahrostami, S.; Zheng, T.; Hu, Y.; Hwang, S.; Stavitski, E.; Peng, Y.; Dynes, J.; Gangisetty, M.; Su, D.; Attenkofer, K.; Wang, H. Energy Environ Sci 2018, 11, 893-903.